Image Cover Sheet

CLASSIFICATION	SYSTEM NUMBER
UNCLASSIFIED	510322

TITLE

BUCKLING AND POST-BUCKLING OF STIFFENED SHELL STRUCTURES USING A CO-ROTATIONAL FINITE ELEMENT FORMULATION

System Number:

Patron Number:

Requester:

Notes: Paper #17 contained in Parent Sysnum #510305

DSIS Use only:

Deliver to: DK

Buckling and Post-buckling of Stiffened Shell Structures Using a Co-rotational Finite Element Formulation

L. Jiang and M.W. Chernuka

Martec Limited, Suite 400, 1888 Brunswick Street
Halifax, Nova Scotia, B3J 3J8

Accurate predictions of the buckling loads and the post-buckling responses of stiffened shell structures are of particular interest in submarine design. In this paper, a co-rotational, updated Lagrangian finite element formulation is presented for geometrically nonlinear structural analysis. This formulation has been incorporated into all the plate/shell and beam elements in the general purpose finite element program VAST along with a group of advanced solution techniques including the displacement control and Crisfield's arc-length methods. In finite element analyses using VAST, stiffened shells can be modelled by either combining compatible shell and beam elements or employing the newly developed stiffened shell element. In the former, beam elements must coincide with shell element edges, whereas in the latter, beam stiffeners are permitted to be located anywhere inside the shell element. Both finite element models have been used to investigate the buckling and post-buckling behaviour of various ring stiffened cylindrical shells under hydrostatic loading. Special emphasis is placed on the sensitivity of geometric imperfections. Excellent numerical solutions have been obtained in the present study.

BUCKLING AND POST-BUCKLING OF STIFFENED SHELL STRUCTURES USING A COROTATIONAL FINITE ELEMENT FORMULATION

Lei JIANG and Michael W. CHERNUKA
Martec Limited, Suite 400, 1888 Brunswick Street, Halifax, Nova Scotia, Canada B3J 3J8

Introduction

Accurate predictions of the buckling loads and post-buckling responses of stiffened shell structures are of particular interest in submarine design. Although the critical load levels can be obtained by using linearized buckling analyses, some deficiencies should be noted. In particular, critical loads may be significantly overestimated if the structure has a highly nonlinear pre-buckling deformation and the sensitivity of the structural collapse to geometric imperfections cannot be studied properly. To obtain post-buckling responses, which are normally characterized by large displacements and rotations, a fully nonlinear finite element formulation has to be employed.

Among the approaches proposed for nonlinear finite element analysis, the most commonly used are the total and updated Lagrangian formulations [1,2]. However, for a special class of nonlinear problems, in which displacements and rotations could be arbitrarily large, but strains are of moderate magnitude, the Lagrangian formulations can be further simplified without significant loss in accuracy. Theoretically, the motion of a continuous medium can always be decomposed into a rigid body motion followed by a pure deformation. The rigid body motion is not involved in the constitutive equation, whereas the pure deformation is not involved with geometric nonlinearities. For problems with arbitrarily large displacements and rotations but small strains, the pure deformation part extracted from the total displacement field is always a small quantity compared with the element dimensions. As a result, the linear finite element theory can be used in element local coordinate systems. Direct separation of the total displacements into its rigid body motion and pure relative deformation components can be accomplished by using a corotational formulation.

The corotational concept has been adopted by several authors in the development of efficient algorithms for geometrically nonlinear analysis of shell structures [3-8]. In the present study, a corotational, updated Lagrangian procedure is developed, in which the element tangent stiffness matrices are generated as in the standard updated Lagrangian formulation [2]; whereas the corotational approach is employed to update element strains, stresses and internal force vectors in the incremental-iterative solution procedure [9-14]. One of the major difficulties in geometrically nonlinear analysis of shells is associated with the non-vectorial characteristic of finite rotations [15].

Several methods have been proposed for updating element geometry and calculating the deformational rotations [6,8]. In our work, the procedure proposed by Rankin and Brogan [8] is followed.

The present corotational procedure is very simple and ideally suited for implementation in existing general purpose linear finite element programs, like VAST [16]. Its effectiveness, robustness and reliability have been demonstrated by a large number of highly nonlinear test problems. In this paper, we will focus on nonlinear analysis of stiffened and unstiffened cylindrical shells, which are often used as simplified test models of submarine pressure hulls.

Nonlinear Finite Element Formulation

Using the principle of virtual work and in the finite element context, the discretized equilibrium equation can be expressed as [1,2]:

$$F({}^tU) - {}^t\lambda P = 0 \tag{1}$$

where **U** indicates the generalized nodal displacement vector. For shell elements, **U** contains both nodal translational displacements, **u**, and rotational variables, θ. **F** is the internal force vector which is a nonlinear function of the generalized nodal displacements. **P** denotes a reference external load vector and λ is a load parameter which controls the actual magnitude of external load. In eqn (1), a proportional conservative loading condition is assumed. In case of nonconservative loading, **P** is also a nonlinear function of the generalized nodal displacements. The left superscript (t) denotes a typical load level.

Incremental-iterative solution algorithms are normally employed to solve the nonlinear equilibrium equations (1). For a typical iteration, (k), in the load step from $(t-\Delta t)$ to (t), the nonlinear equations can be linearized using the Newton-Raphson method as:

$$K_T({}^tU^{(k-1)})\,\Delta U = ({}^t\lambda^{(k-1)} + \Delta\lambda)P - F({}^tU^{(k-1)}) \tag{2}$$

where $\mathbf{K_T}$ is the tangent stiffness matrix. ${}^tU^{(k-1)}$ and ${}^t\lambda^{(k-1)}$ indicate the total generalized nodal displacements and load parameter obtained at the end of the previous iteration, whereas $\Delta\mathbf{U}$ and $\Delta\lambda$ are the incremental displacements and load parameter for the current iteration.

To solve eqn (2) for $\Delta\mathbf{U}$ and $\Delta\lambda$, an additional constraint equation has to be specified in the solution space. The commonly used constraint equations include the constant load incrementation [1,2], the displacement control [17] and the arc-length method [18]. In the constant load

incrementation method, a load increment, which is indicated by a left subscript 't', is specified at the beginning of a load step as:

$$ {}_t\lambda = {}^t\lambda - {}^{t-\Delta t}\lambda \tag{3} $$

and kept as constant during the Newton-Raphson iterations as shown in Fig. 1(a). Although this constraint equation is adequate for a wide range of nonlinear engineering problems, convergence difficulties may occur in the vicinity of load limit points. This numerical difficulty can be overcome by employing the constant arc-length constraint, defined as:

$$ \left({}_t\mathbf{U}^{(k-1)} + \Delta \boldsymbol{U} \right)^T \left({}_t\boldsymbol{U}^{(k-1)} + \Delta \boldsymbol{U} \right) + \left({}_t\lambda^{(k-1)} + \Delta\lambda \right)^2 = \Delta\ell^2 , \tag{4} $$

by which the equilibrium state $({}^t\mathbf{U}, {}^t\lambda)$ is approached on a cylindrical surface in the solution space and the load limit points can then be passed easily as shown in Fig. 1(b).

After each iteration, the accumulated load parameter and translational displacement increments in the current load step can be updated as:

$$ {}_t\lambda^{(k)} = {}_t\lambda^{(k-1)} + \Delta\lambda \quad \text{and} \quad {}_t\boldsymbol{u}^{(k)} = {}_t\boldsymbol{u}^{(k-1)} + \Delta\boldsymbol{u} \tag{5} $$

and the total load parameter and nodal translations updated as:

$$ {}^t\lambda^{(k)} = {}^{t-\Delta t}\lambda + {}_t\lambda^{(k)} \quad \text{and} \quad {}^t\boldsymbol{u}^{(k)} = {}^{t-\Delta t}\boldsymbol{u} + {}_t\boldsymbol{u}^{(k)} \tag{6} $$

where ${}^{t-\Delta t}\lambda$ and ${}^{t-\Delta t}\boldsymbol{u}$ indicate the converged solution obtained for the previous load step. Sophisticated large rotation theory [15] is required when updating the nodal rotational variables.

Corotational Procedure

In order to describe the corotational procedure, three Cartesian coordinate systems have to be defined. They are:

i) The global coordinate system, **G**;

ii) The element corotational coordinate system, **E**, which is associated with each element and undergoes rigid body rotations and translations with the element; and

iii) The shell surface coordinate system, $\mathbf{V}_i$, which is the nodal triad associated with node i in a shell or beam element.

As previously mentioned, in the present study, the corotational approach is only employed in the internal force calculation. In order for the linear finite element theory to generate sufficiently accurate results, the pure deformational displacements and rotations employed in internal force calculations must be small quantities relative to the element dimensions. For this reason, it is appropriate to update the reference configuration after each new converged solution has been obtained. By doing this, we are dealing with the increments of the deformational displacements and rotations in the current load step instead of the accumulated ones in the whole deformation process as was done by other investigators [4-7].

Transforming both the internal force vector and the Cauchy stress tensor into the element corotational framework, the linear strain-displacement matrix in the element co-rotational coordinate system can be expressed as:

$$ {}^{t}\tilde{B}_{L} = \Phi({}^{t}E)\ {}^{t}B_{L}\ {}^{t}E \tag{7} $$

where the tilde '~' indicates quantities measured in the corotational coordinate system and Φ is the standard strain transformation matrix, which is a function of **E**.

If the incremental strains are small quantities in each load step, the quadratic terms in the incremental Green-Lagrange strain tensor can be neglected in the element corotational coordinate system and the second Piola-Kirchhoff and the Cauchy stress tensors also become indistinguishable. As a result, the corotational Cauchy stress can be updated approximately using a piece-wise linear strain-displacement relation as:

$$ {}^{t+\Delta t}\tilde{\tau} \approx \tilde{C}\ {}^{t}\tilde{B}_{L}\ \tilde{U}_{def} + {}^{t}\tilde{\tau} \tag{8} $$

where $\tilde{\mathbf{C}}$ indicates the incremental constitutive matrix and $\tilde{U}_{def}$ is the increment of the deformational displacements and rotations in the current load step.

The element internal force vector for the current (t+Δt) configuration can now be evaluated in the global coordinate system as:

$$ {}^{t+\Delta t}f = \int_{{}^{t+\Delta t}V} {}^{t+\Delta t}B_{L}^{T}\ \Phi({}^{t+\Delta t}E)\ {}^{t+\Delta t}\tilde{\tau}\ d^{t+\Delta t}V \tag{9} $$

The integral in (9) is evaluated using numerical integration. The approximate Cauchy stress tensor given in (8) is also employed to calculate the geometric stiffness matrix.

The element-independent corotational approach proposed by Rankin and Brogan [8] is adopted in the present study to extract the deformational part of displacements and rotations. Assuming that

the local co-rotational coordinate system in the latest obtained configuration associated with a typical element rotates to ${}^{t+\Delta t}\mathbf{E}$ from ${}^{t}\mathbf{E}$ in the reference configuration, the deformational translations, $\tilde{\mathbf{u}}_{def}$, and rotation matrix, $\tilde{\mathbf{D}}_i$, can be expressed as:

$$\tilde{u}_{def} = {}^{t+\Delta t}E^T\,({}^tX + {}_tu) - {}^tE^T\,{}^tX \tag{10}$$

and

$$\tilde{D}_i = {}^{t+\Delta t}E^T({}^{t+\Delta t}V_i\,{}^tV_i^T)\,{}^tE. \tag{11}$$

Based on large rotation theory, the pseudo-vector corresponding to the deformational rotations can be obtained through a skew-symmetric matrix defined as:

$$\Omega_i = \frac{2(\tilde{D}_i - \tilde{D}_i^T)}{1+trace\ (\tilde{D}_i)} \tag{12}$$

and used as a part of $\tilde{U}_{def}$ in (8).

Computer Implementation

The present corotational procedure has been implemented for eight elements in our general purpose finite element program, VAST [9-14, 16]. These elements include 8-noded degenerate, isoparametric thick/thin shell (IEC=1); 4-noded quadrilateral shell (IEC=5); 3-noded triangular plate/shell (IEC=4); 3-noded curved beam (IEC=7); 2-noded general beam (IEC=3); 8-noded stiffened shell (IEC=25); 20-noded 3D solid (IEC=2) and 13-noded transition (IEC=6) elements, which are shown graphically in Fig. 2. To alleviate the shear and membrane "locking" problem in isoparametric structural elements, uniformly reduced numerical integration technique is employed in 8-noded thick/thin shell, 8-noded stiffened shell, 3-noded curved beam and 13-noded transition elements and the mixed interpolation formulation of tensorial transverse shear components, initially proposed by Bathe and Dvorkin [19,20], is adopted in 4-noded quadrilateral shell element. Element corotational coordinate systems are calculated using the corner nodes for higher-order finite elements.

Numerical Examples

Example 1: Pre- and Post-buckling of a Cylindrical Shell

In this example, we considered a cylindrical shell with diaphragm ends under uniform pressure as shown in Fig. 3. In order to initiate buckling, a geometric imperfection corresponding to the third buckling mode is imposed on the undeformed configuration according to:

$$\Delta R = \delta \cos(3\psi)\cos\left(\frac{\pi X}{2L}\right) \tag{13}$$

where R is the radius of the cylinder and δ indicates the maximum imperfection. In this example, we took $\delta = 0.005$m. L denotes half length of the cylinder and ψ is measured counterclockwise from the positive Y direction. Due to the symmetry, only a quarter of the whole cylinder was included in our finite element model and discretized into meshes of the 8-noded, 4-noded and 3-noded shell elements, respectively, as shown in Fig. 4. The deformed configurations obtained by using different shell elements are displayed in Figs. 5-7 and the load-deflection curves are compared in Fig. 8, where node A (see Fig. 4) is the one having maximum total deflection in the symmetric plane X=0. The nonconservative characteristic of hydrostatic pressure was taken into account. Both the critical load levels and the post-buckling responses predicted by these three shell elements are in good agreement.

Example 2: Pre- and Post-buckling of a Stiffened Cylindrical Shell

In the second example, we considered two simplified test models of a submarine pressure hull, which are cylindrical shells reinforced by four ring stiffeners, as shown in Fig. 9. These test models have diaphragms at both ends and are subjected to uniform hydrostatic pressure. When the stiffeners are weak compared with the shell and the nonlinear pre- and post-buckling response is dominated by the shell stiffness, an overall buckling mode is produced. On the other hand, when the stiffeners are stiff compared with the shell, the lowest buckling load is associated with a interframe buckling mode.

For the overall buckling model, we imposed the same geometric imperfection on the undeformed configuration as in the previous example. Making use of the symmetry condition, a quarter of the shell was discretized into 8x10 and 12x10 finite element meshes as shown in Fig. 10, where the shell was modelled by 8-noded thick/thin shell elements and the stiffeners by 3-noded curved beam elements. Deformed configurations obtained using the finer finite element model are shown in Fig. 11 and the load-deflection curves obtained by VAST are

compared with the ADINA solution [21] in Fig. 12. Good agreement between VAST and ADINA solutions are observed.

To initiate buckling in the interframe buckling model, a geometric imperfection corresponding to the seventh buckling mode was imposed and a very coarse 7x10 finite element mesh was employed to model a quarter of the structure (see Fig. 13). The final deformed configuration is shown in Fig. 14, where the "interframe buckling" deformations are clearly demonstrated. The load-deflection curve is compared to ADINA solution in Fig. 15 with good agreement.

Example 3: Structure's Sensitivity to Geometric Imperfections

In the last example, we considered another stiffened cylindrical shell as shown in Fig. 16. It is similar to the one in the previous example. However, the primary focus for this example is the effect of geometric imperfections on the critical load and the nonlinear pre- and post-buckling responses of the structure. Using our newly developed 8-noded stiffened shell element (see Fig. 2(f)), in which stiffeners are permitted to locate arbitrarily, three finite element models were generated containing one-eighth of the shell, as shown in Fig. 17, where the solid lines indicate the boundaries of the stiffened shell elements and the dashed lines indicate the locations of the stiffeners.

Geometric imperfections corresponding to the fourth buckling mode and having maximum magnitudes of 10%, 30% and 50% of the shell thickness were imposed on each of these three finite element models. A group of linearized buckling analyses were carried out and the first critical loads obtained for each case are summarized in Table 1. However, the effect of geometric imperfections were not apparent . This is due to the limitation of the linearized buckling analysis method for problems with highly nonlinear pre-buckling deformation. Using the corotational, updated Lagrangian formulation presented in this paper, the sensitivity of the structure to geometric imperfections can be directly observed from the load-deflection curves in Fig. 18, where the good agreement between the results obtained using different meshes indicates the convergence of the nonlinear solution. The final deformed configuration obtained using the finest mesh and the smallest geometric imperfection is displayed in Fig. 19.

Conclusion

A simple corotational, updated Lagrangian formulation has been presented for geometrically nonlinear analysis with arbitrarily large displacements and rotations. In this formulation, the element strain, stress and internal force vectors are updated using a corotational approach, whereas the tangent stiffness matrices are evaluated using a standard updated Lagrangian formulation. The use of a piece-wise linear strain-displacement relation permits the element strains to be in moderate range. The non-vectorial characteristic of large rotations was taken into account when updating total deformation and extracting the pure deformational rotations. The current nonlinear formulation is ideally suited for implementation in existing linear finite element programs and has been incorporated in eight most commonly used elements of VAST. In this paper, the effectiveness and robustness of the nonlinear capability in VAST have been demonstrated through a set of buckling analyses of geometrically imperfect, stiffened and unstiffened, cylindrical shells, for which the linearized buckling analysis is normally inadequate.

References

1. O.C. Zienkiewicz, *The Finite Element Method*, 3rd Edn. McGraw-Hill, London (1977).
2. K.J. Bathe, *Finite Element Procedures in Engineering Analysis*, Prentice-Hall, New Jersey (1982).
3. T. Belytschko and B.J. Hsieh, Nonlinear Transient Finite Element Analysis with Convected Coordinates. *Int. J. Numer. Meth. Engng.* **7**, 255-271 (1973).
4. G. Horrigmoe and P.G. Bergan, Nonlinear Analysis of Free-form Shells by Flat Finite Elements. *Comput. Meth. Appl. Mech. Engng.* **16**, 11-35 (1978).
5. S. Oral and A. Barut, A Shear-flexible Facet Shell Element for Large Deflection and Instability Analysis. *Comput. Meth. Appl. Mech. Engng.* **93**, 415-431 (1991).
6. K.M. Hsiao, Nonlinear Analysis of General Shell Structures by Flat Triangular Shell Element. *Comput. Struct.* **25**, 665-675 (1987).
7. K.M. Hsiao and H.C. Hung, Large-deflection Analysis of Shell Structure by Using Corotational Total lagrangian Formulation. *Comput. Meth. Appl. Mech. Engng.* **73**, 209-225 (1989).
8. C.C. Rankin and F.A. Brogan, An Element Independent Corotational Procedure for the Treatment of Large Rotations. *J. Press. Vessel Technol. ASME* **108**, 165-174 (1986).

9. L. Jiang and M.W. Chernuka, *Implementation of a Large Displacement Capability for VAST - Phase I.* Martec Technical Report TR-91-28, Martec Limited, Halifax, Nova Scotia (1991).
10. L. Jiang and M.W. Chernuka, *Implementation of a Large Displacement Capability for VAST - Phase II.* Martec Technical Report (under preparation), Martec Limited, Halifax, Nova Scotia (1993).
11. L. Jiang, M.W. Chernuka and N.G. Pegg, A Corotational Updated Lagrangian Formulation for Geometrically Nonlinear Finite Element Analysis. *Finite Elements in Analysis and Design* (in press) (1993).
12. L. Jiang and M.W. Chernuka, A Corotational Formulation for Geometrically Nonlinear Finite Element Analysis of Spatial Beams. *Tran. CSME* (submitted) (1993).
13. L. Jiang and M.W. Chernuka, A Simple Four-noded Corotational Shell Element for Arbitrarily Large Rotations. *Comput. Struct.* (submitted) (1993).
14. L. Jiang and M.W. Chernuka, An Eight-noded Stiffened Shell Element with Geometrically Nonlinear Capability. *Eng. Comput.* (under preparation) (1993).
15. J.H. Argyris, An Excursion into Large Rotations. *Comput. Meth. Appl. Mech. Engng.* **32**, 85-155 (1982).
16. *VAST User's Manual*, Version 6.0, Martec Limited, Halifax, Nova Scotia, Canada (1992).
17. J.L. Batoz and G. Dhatt, Incremental Displacement Algorithms for Nonlinear Problems. *Int. J. Numer. Meth. Engng.* **14**, 1262-1266 (1979).
18. M.A. Crisfield, A Fast Incremental/iterative Solution Procedure that Handles "Snap-through". *Comput. Struct.* **13**, 55-62 (1981).
19. E.N. Dvorkin and K.J. Bathe, A Continuum Mechanics Based Four-node Shell Element for General Nonlinear Analysis. *Eng. Comput.* **1**, 77-88 (1984).
20. K.J. Bathe and E.N. Dvorkin, A Formulation of General Shell Elements — the Use of Mixed Interpolation of Tensorial Components. *Int. J. Numer. Meth. Engng.* **22**, 697-722 (1986).
21. S.C. Burrell and M.W. Chernuka, *Submarine Pressure Hull Buckling Models*, Martec Technical Report TR-89/90-06G, Martec Limited, Halifax, Nova Scotia (1990).

Mesh	Geometric Imperfection			
	0%	10%	30%	50%
4x5	38.725	38.812	38.949	39.017
5x6	39.213	39.319	39.478	39.564
7x8	39.185	39.296	39.458	39.548

(Reference pressure load = 10^5 N/m^2)

Table 1 First critical load predicted by the linearized buckling analysis for different meshes and geometric imperfections.

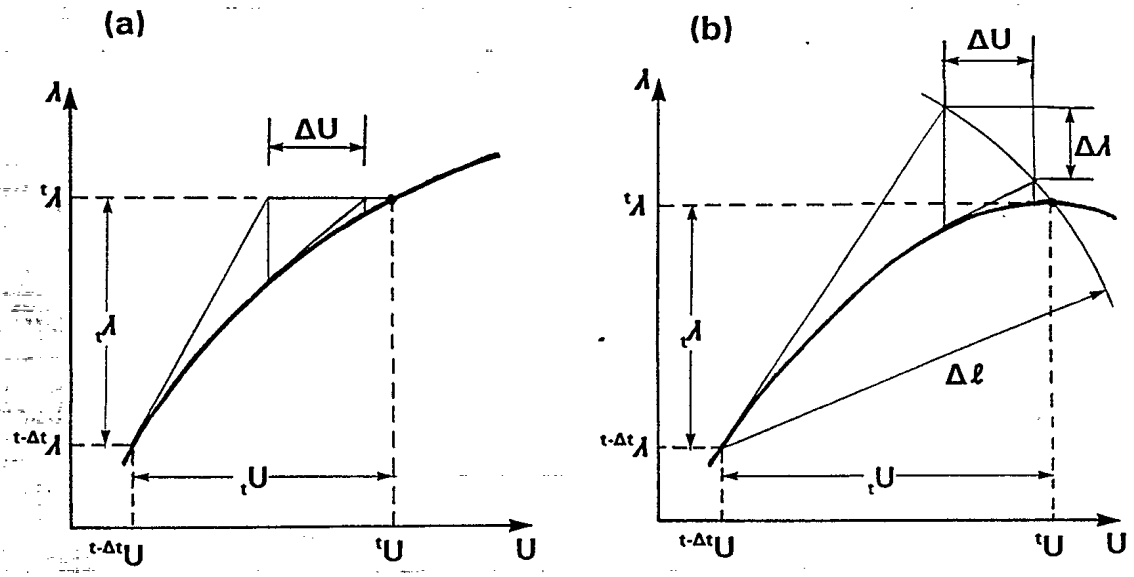

Fig. 1 Incremental-iterative solution procedure for nonlinear finite element equations.

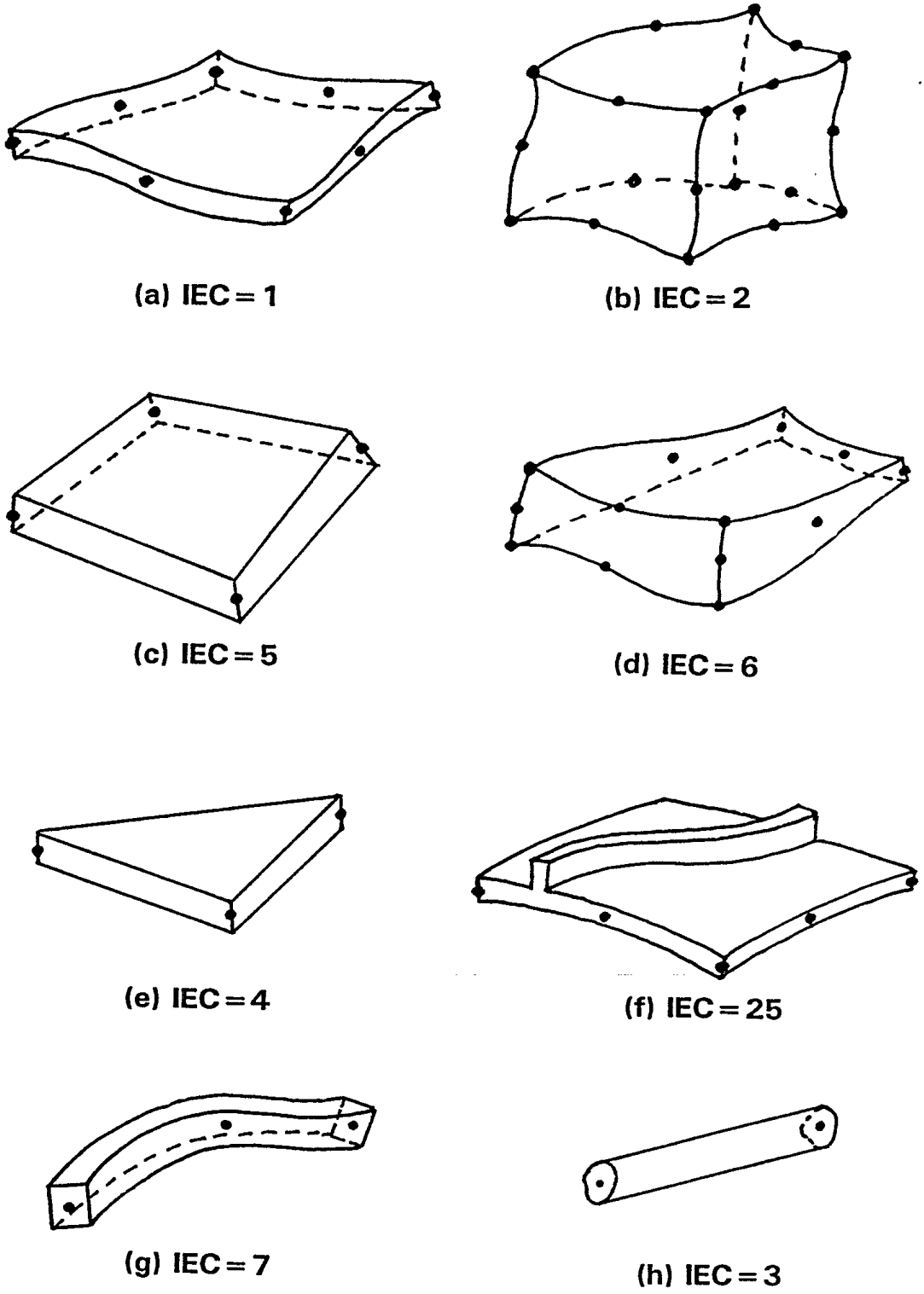

Fig. 2 Nonlinear element library of VAST 7.0.

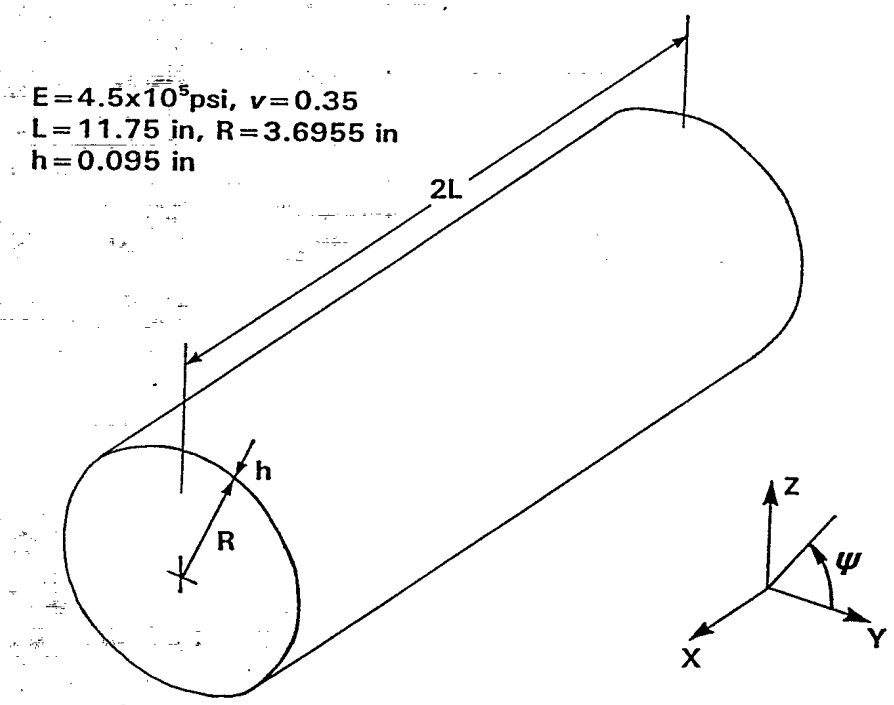

Fig. 3 Problem geometry and material properties of a diaphragmed cylindrical shell.

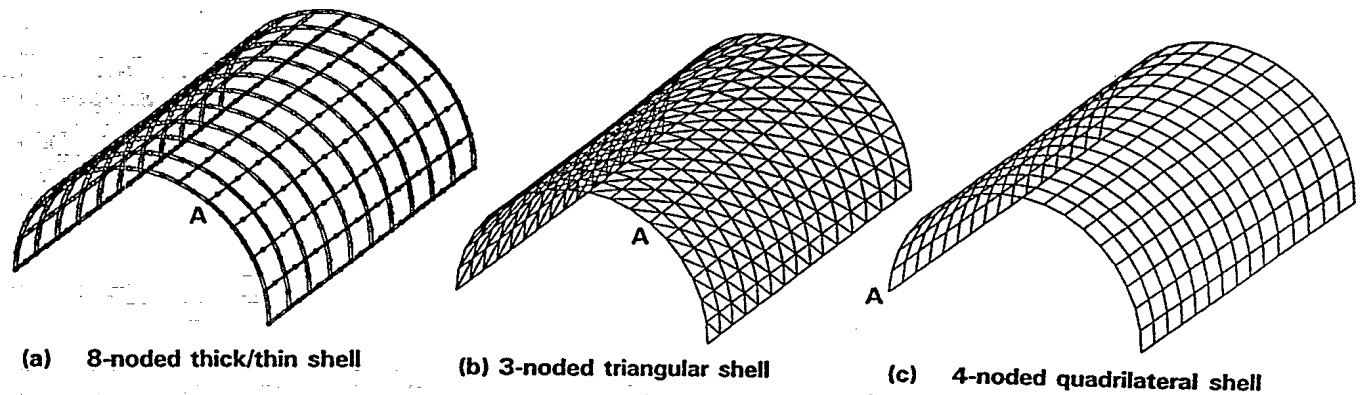

Fig. 4 Finite element models for buckling analysis of the cylindrical shell.

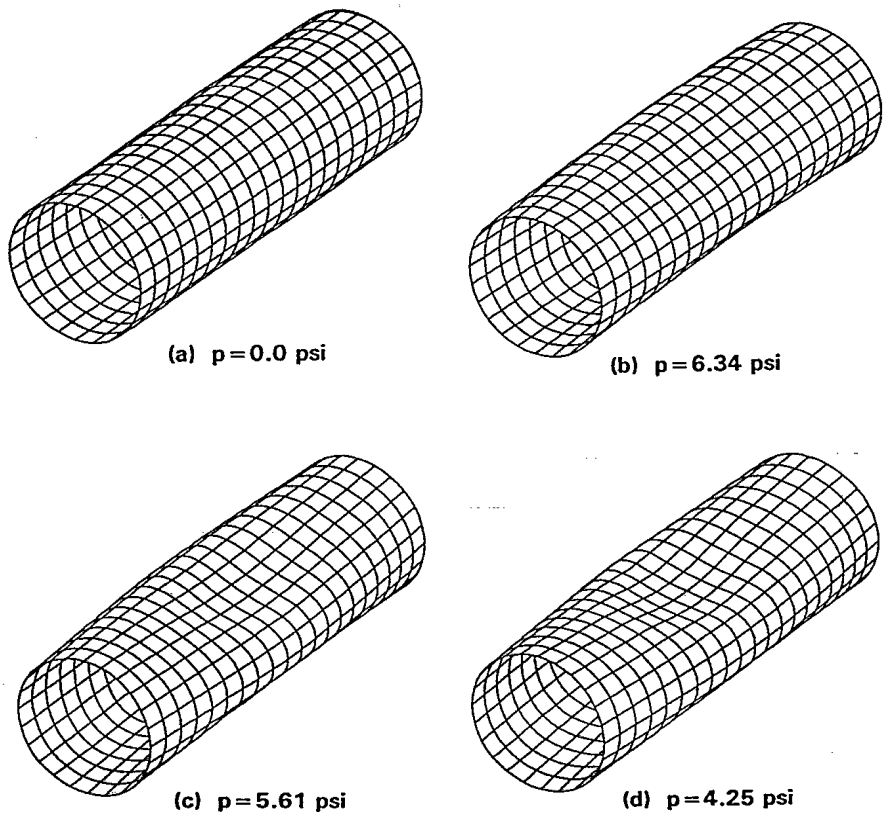

Fig. 5 Deformed configurations of the cylindrical shell obtained using 8-noded shell elements.

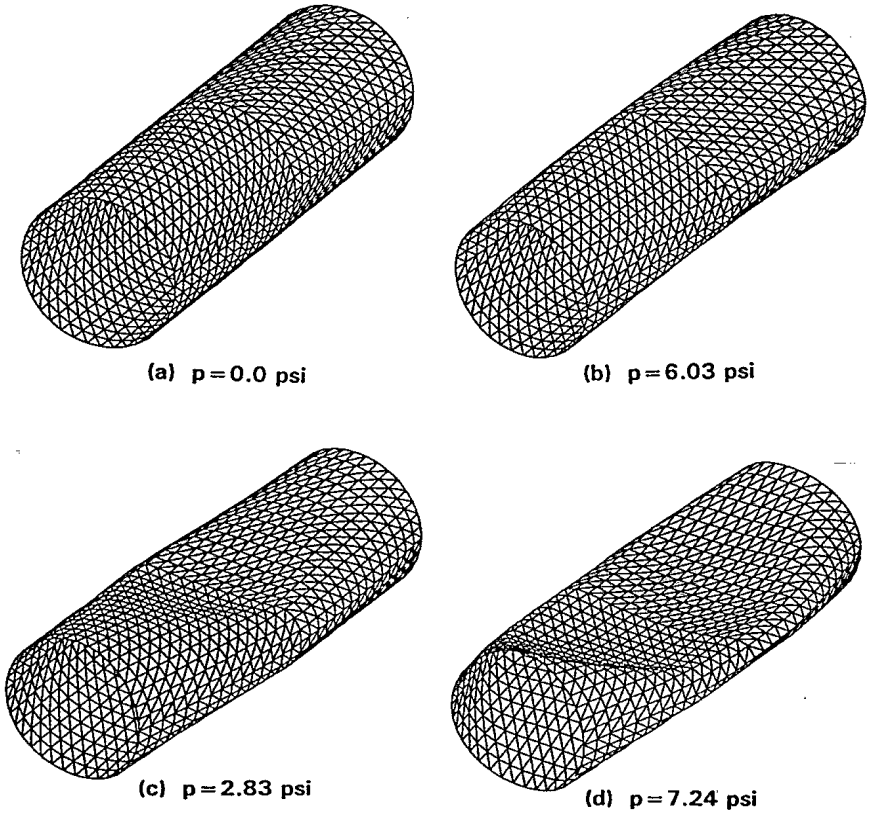

Fig. 6 Deformed configurations of the cylindrical shell obtained using 3-noded shell elements.

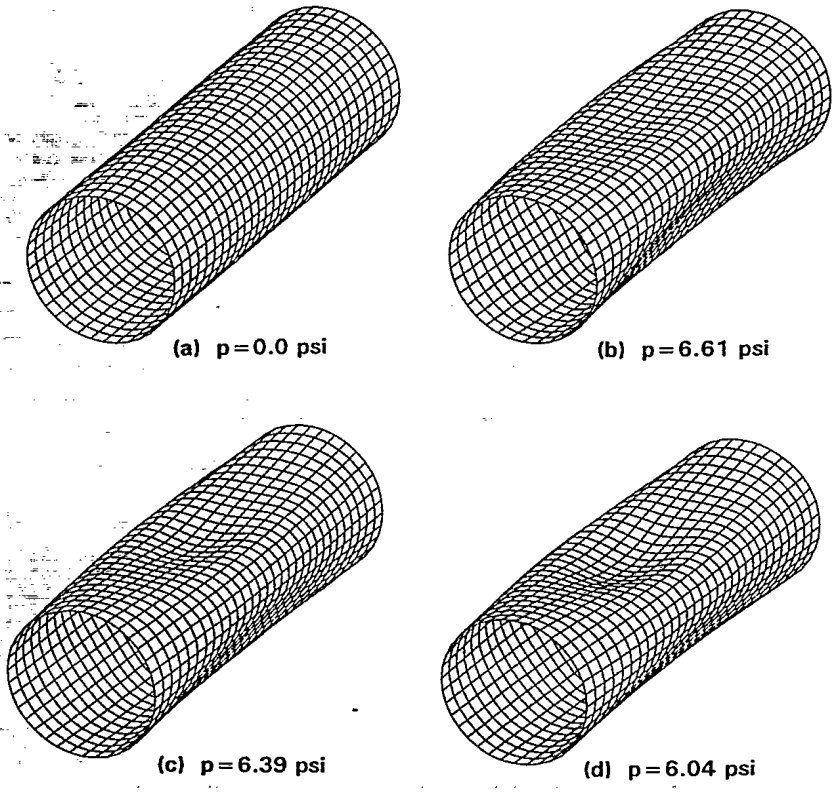

Fig. 7 Deformed configurations of the cylindrical shell obtained using 4-noded shell elements.

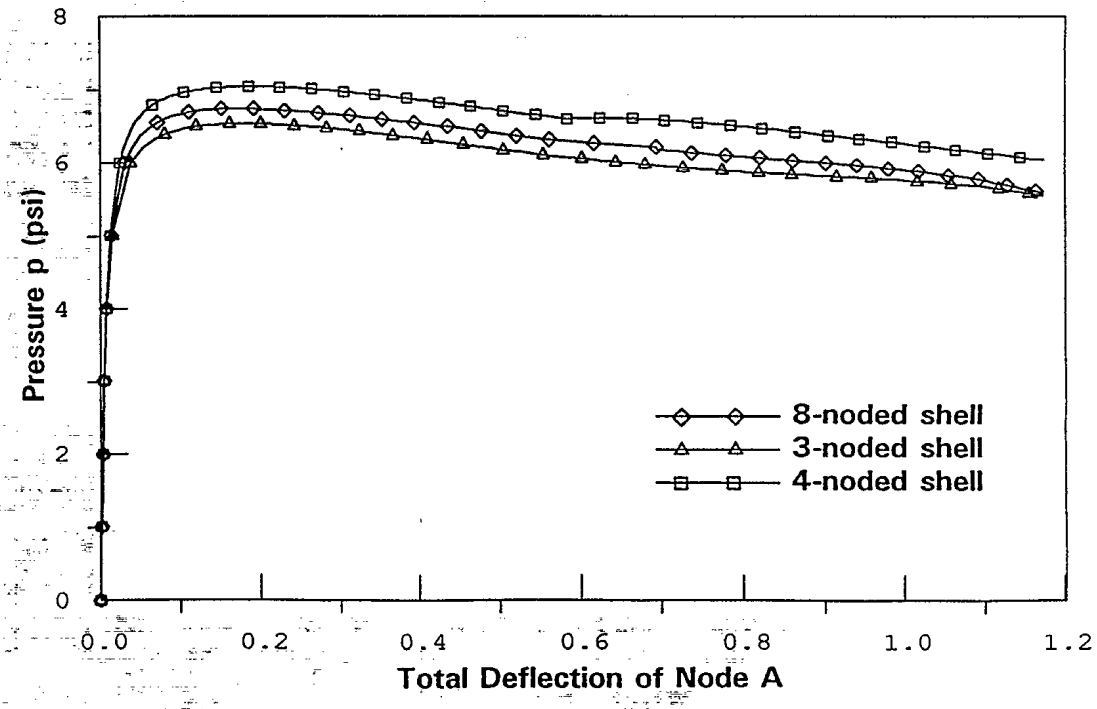

Fig. 8 Comparison of load-deflection curves obtained using different shell element models.

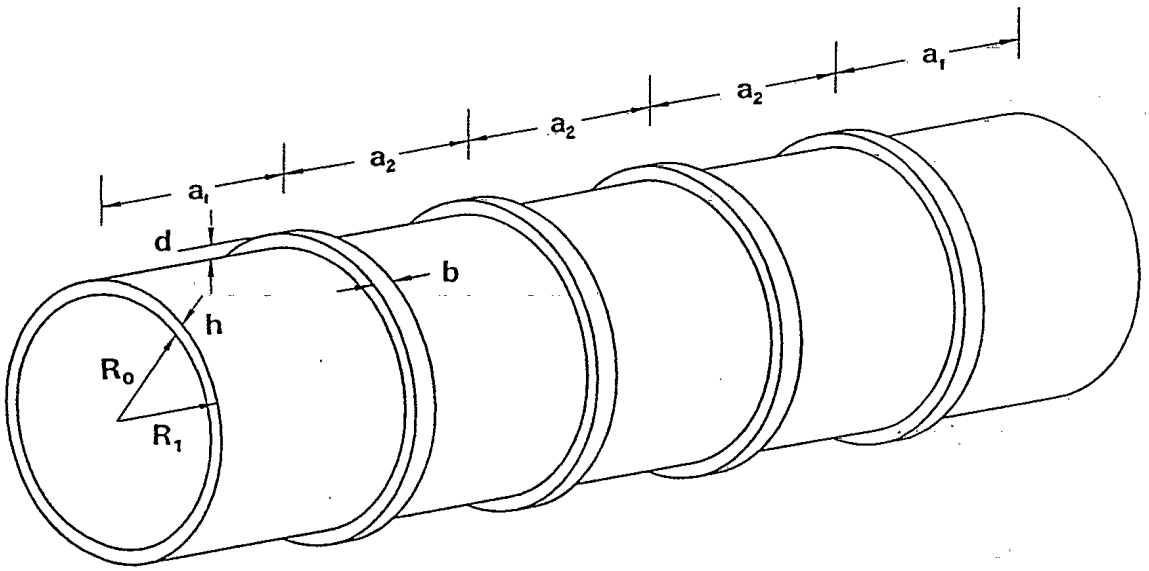

$E = 4.5 \times 10^5$ psi, $\nu = 0.35$
$a_1 = 5.0$ in, $a_2 = 4.5$ in, $R_o = 3.648$ in

For overall buckling model:

$R_1 = 3.743$ in, $h = 0.095$ in
$b = d = 0.1$ in

For interframe buckling model:

$R_1 = 3.7$ in, $h = 0.052$ in
$b = 0.25$ in, $d = 0.4$ in

Fig. 9 Problem geometry and material properties of diaphragmed stiffened cylindrical shells.

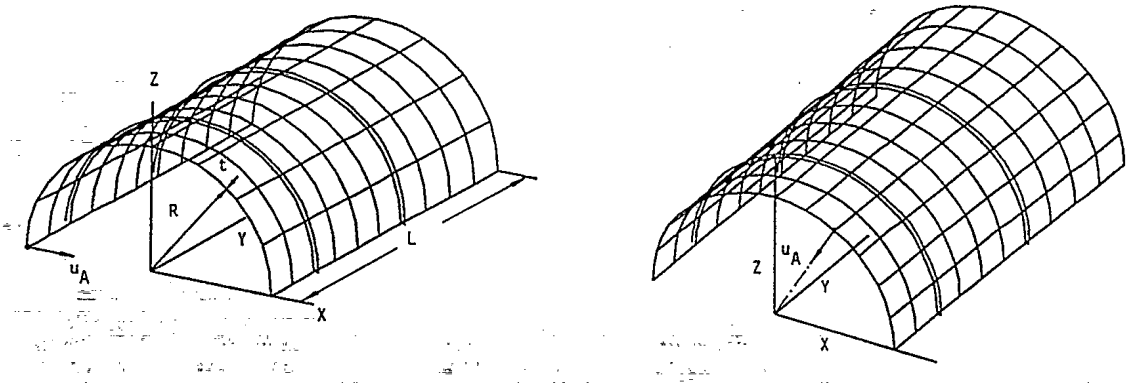

(a) 8x10 mesh (b) 12x10 mesh

Fig.10 Finite element meshes of buckling analysis of the overall buckling model.

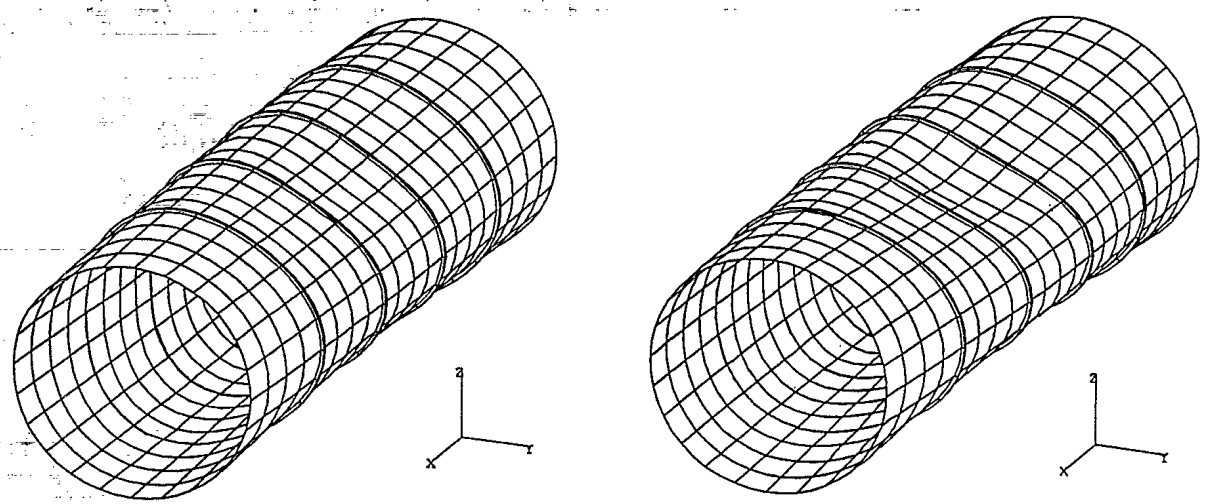

(a) p = 8.98 psi (b) p = 8.14 psi

Fig.11 Deformed configurations of the overall buckling model obtained using the finer mesh.

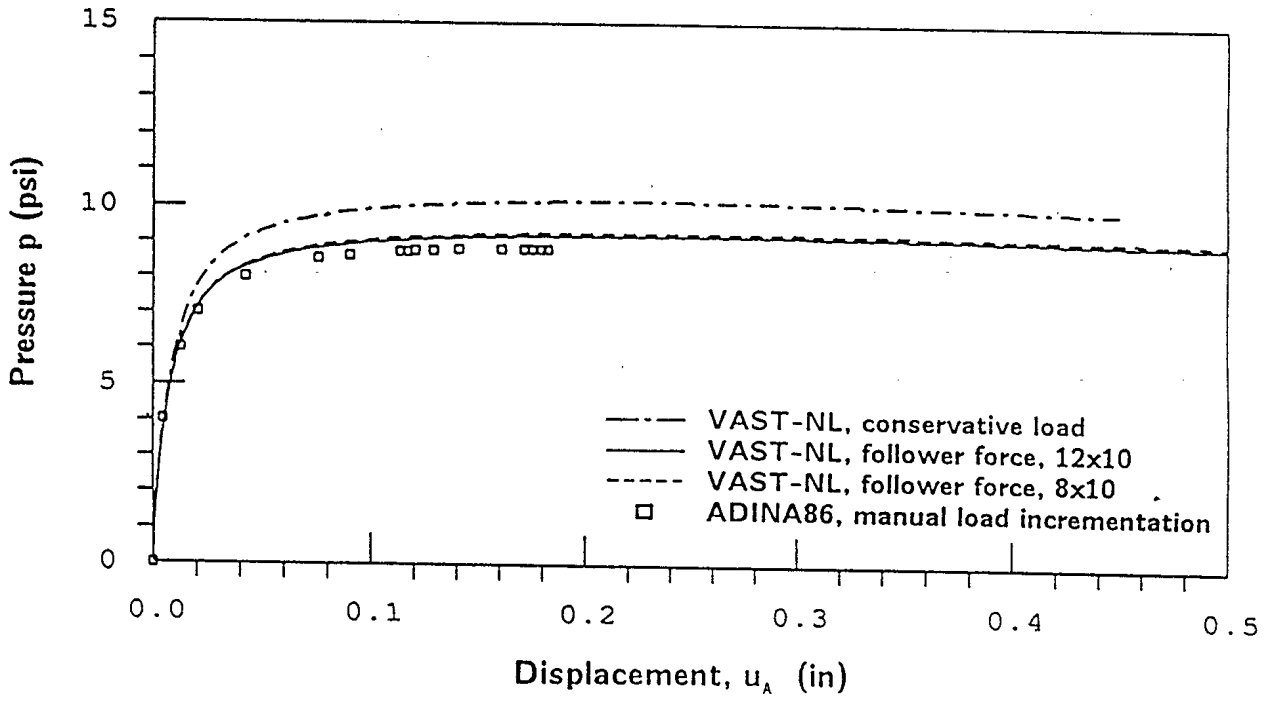

Fig.12 Comparison of load-deflection curves obtained by VAST 7.0 and ADINA for the overall bucking model.

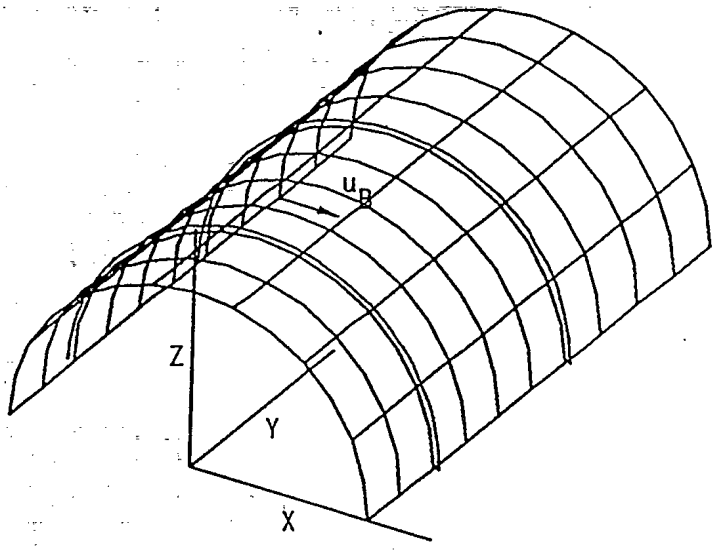

Fig.13 Finite element mesh for the interframe buckling model.

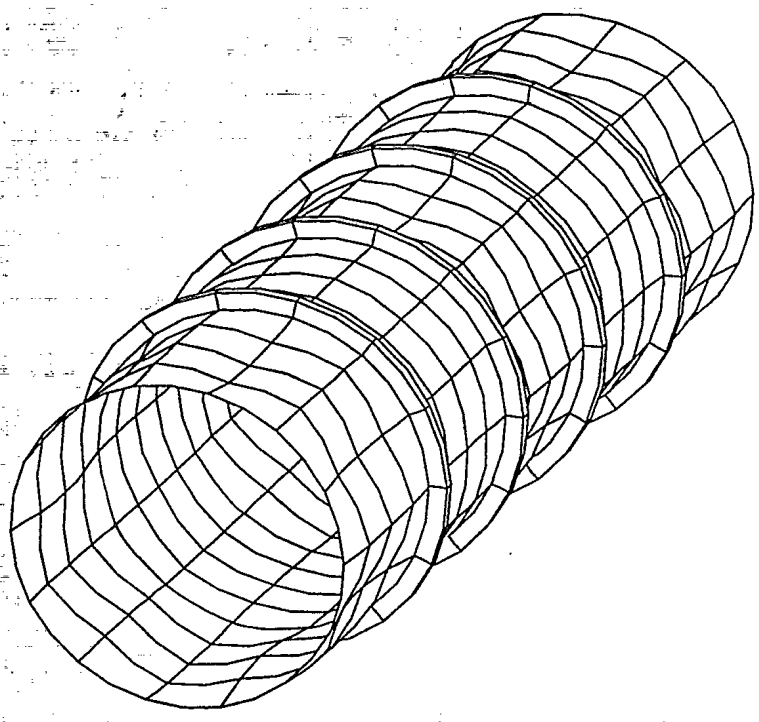

Fig.14 Final deformed configuration (p=10.44 psi) of the interframe buckling model.

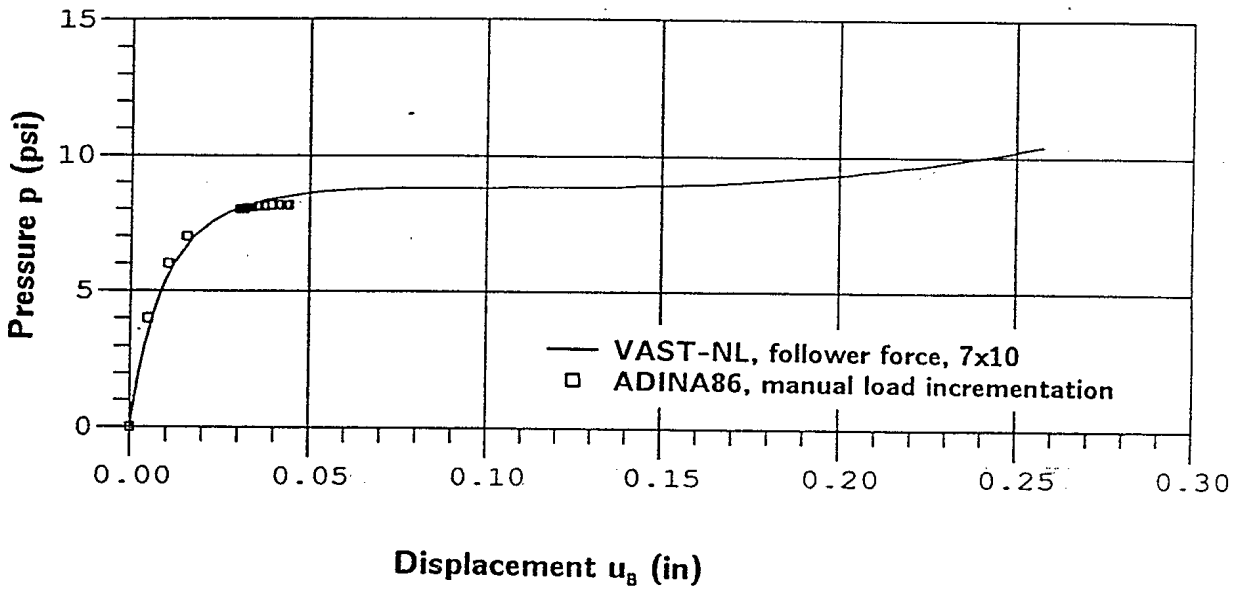

Fig.15 Comparison of load-deflection curves obtained by VAST 7.0 and ADINA for the interframe bucking model.

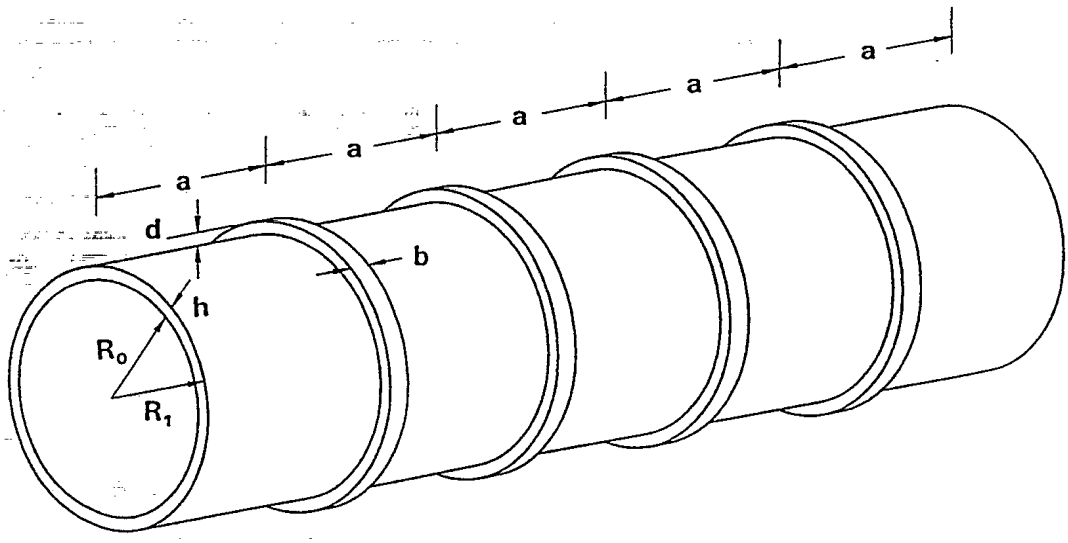

Fig.16 Problem geometry and material properties of a stiffened cylindrical shell used for investigating structure's sensitivity to geometric imperfections.

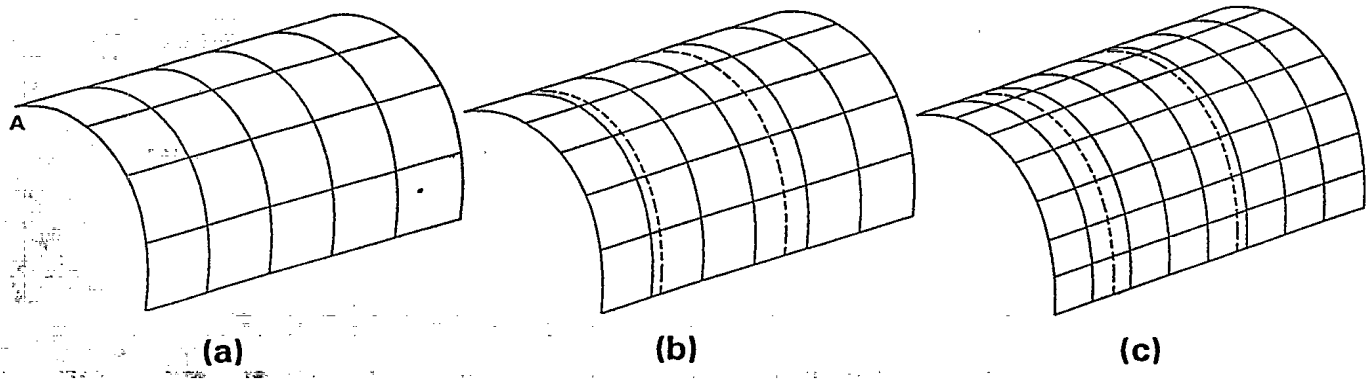

Fig.17 Finite element models of the stiffened shell elements. (a) 4x5, (b) 5x6, (c) 7x8.

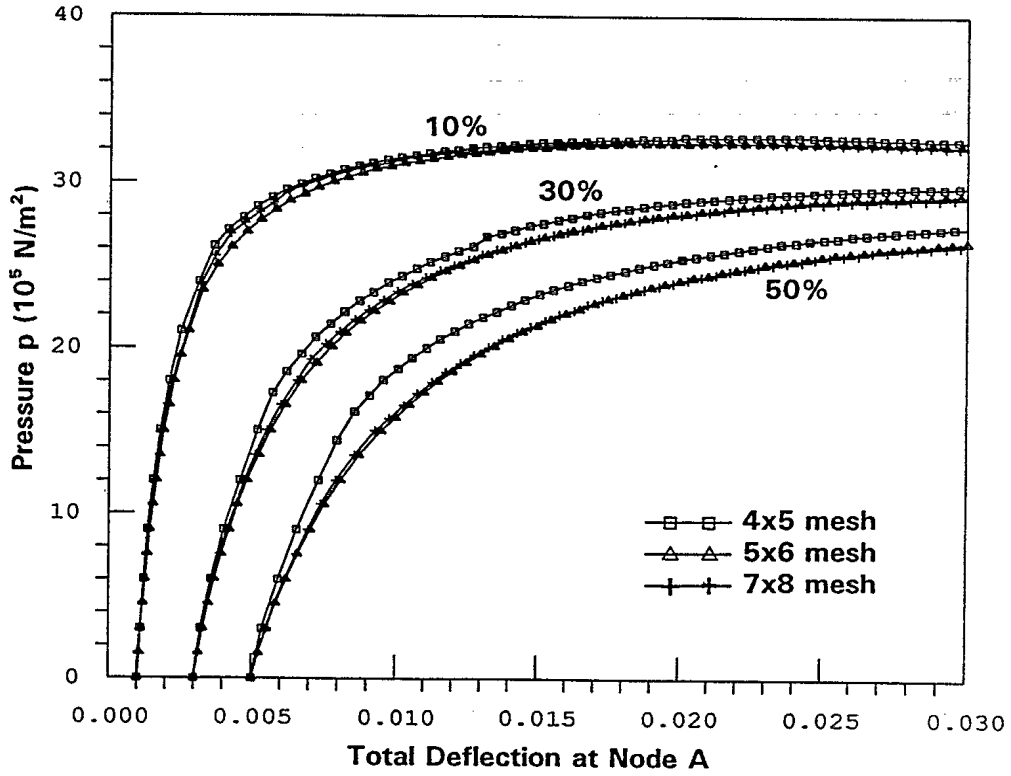

Fig.18 Comparison of load-deflection curves obtained by using different finite element meshes and amount of geometric imperfections.

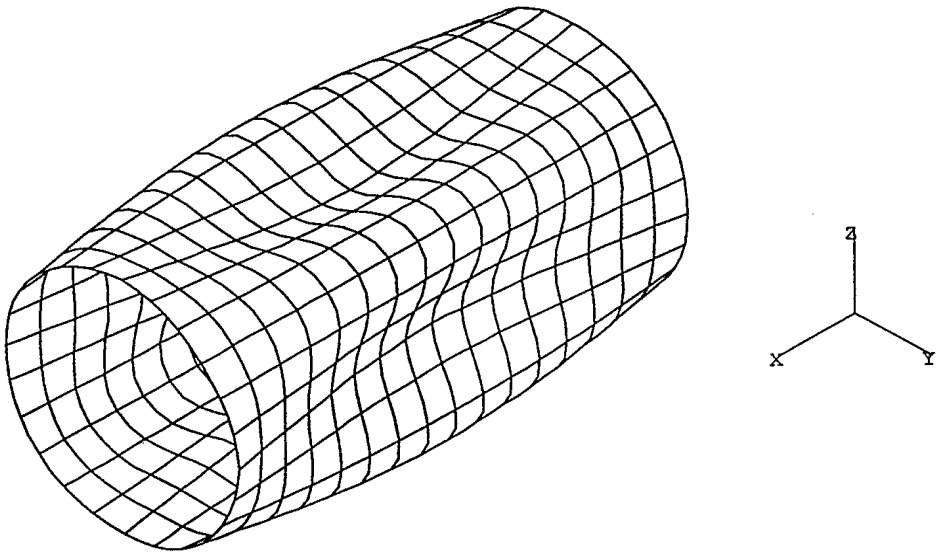

Fig.19 Final deformed configuration ($p=3.21\times10^6$ N/m^2) obtained by using the finest mesh and 10 percent of geometric imperfection.